Integration of Zn-Ag and Zn-air Batteries: A Hybrid Battery with the Advantages of Both

Peng Tan,[◊,†] Bin Chen,[†] Haoran Xu,[†] Weizi Cai,[†] Wei He,[†] Houcheng Zhang,[†,Δ] Meilin Liu,[‡] Zongping Shao,[§,∥] Meng Ni*[†,#]*

◊ Department of Thermal Science and Energy Engineering, University of Science and Technology of China, Hefei 230026, China

† Department of Building and Real Estate, The Hong Kong Polytechnic University, Hung Hom, Kowloon, Hong Kong 999077, China

Δ Department of Microelectronic Science and Engineering, Ningbo University, Ningbo 315211, China

‡ School of Materials Science and Engineering, Center for Innovative Fuel Cell and Battery Technologies, Georgia Institute of Technology, Atlanta, GA 30332-0245, USA

§ Jiangsu National Synergetic Innovation Center for Advanced Material, College of Energy, State Key Laboratory of Materials-Oriented Chemical Engineering, Nanjing Tech University, Nanjing 210009, China

∥ Department of Chemical Engineering, Curtin University, Perth, WA 6845, Australia

Environmental Energy Research Group, Research Institute for Sustainable Urban Development (RISUD), The Hong Kong Polytechnic University, Hung Hom, Kowloon, Hong Kong 999077, China

KEYWORDS: Zn-air battery, Zn-Ag battery, hybrid system, energy efficiency, cycling stability

ABSTRACT: We report a hybrid battery that integrates a Zn-Ag battery and a Zn-air battery to utilize the unique advantages of both battery systems. In the positive electrode, Ag nanoparticles couple the discharge behaviors through the two distinct electrochemical systems by working as the active reactant and the effective catalyst in the Zn-Ag and Zn-air reactions, respectively. In the negative electrode, in-situ grown Zn particles provide large surface areas and suppress the dendrite, enabling the long-term operating safety. The battery first exhibits two-step voltage

plateaus of 1.85 V and 1.53 V in the Zn-Ag reaction, after which a voltage plateau of 1.25 V is delivered in the Zn-air reaction, and the specific capacity reaches 800 mAh g_{Zn}^{-1}. In addition, excellent reversibility and stability with maintaining high energy efficiency of 68% and capacity retention of nearly 100% at 10 mA cm^{-2} are demonstrated through 100 cycles, outperforming both conventional Zn-air and Zn-Ag batteries. This work brings forth a conceptually novel high-performance battery, and more generally opens up new vistas for developing hybrid electrochemical systems by integrating the advantages from two distinct ones.

1. Introduction

Advanced power systems with high energy densities are the key to electric vehicles and portable electronic devices.[1] Although today's lithium-ion batteries present high discharge voltage, good energy efficiency, and long cycle life,[2] their energy densities (~400 Wh kg^{-1}) are still insufficient for the demand.[3] To this end, great efforts have been made in the explorations of other energy conversion/storage systems, for example, fuel cells, supercapacitors, and novel battery systems.[4,5] Research interest has been made in Zn-based rechargeable batteries (e.g., Zn-MnO_2 and Zn-Ni batteries),[6,7] owing to the remarkable electrochemical performance, high safety, and low cost.[8] Among them, Zn-Ag batteries, one of the most mature battery systems that can be used in both small scale (e.g., watches) and large scale (e.g., military and aerospace) applications, hold great promise as high-performance, safe, and environment-friendly power sources.[9] They can deliver high operating voltages up to 1.85 V, and exhibit the continuous power densities up to 600 W kg^{-1} and pulsed power densities up to 2500 W kg^{-1}.[10] However, neither the energy density (~300 Wh kg^{-1}) nor the cycle life of Zn-Ag batteries are sufficient for many applications.[11] Other concerns include Zn dendrite formation, separator degradation,[10] and

oxygen evolution at high charging voltages (~1.7 V vs. Zn), which not only affects the charging efficiency of Ag, but also threatens the operating safety.[12]

The limited capacity of closed battery systems has prompted the development of metal-air battery systems. For example, Zn-air batteries with an open-air electrode (that uses oxygen from ambient air without adding mass to or occupying volume of the battery) have a theoretical energy density of 1218 Wh kg^{-1}.[13] In addition to the oxidation and reduction of Zn during discharge and charge, the working mechanisms of a rechargeable Zn-air battery involve the oxygen reduction reaction (ORR) and evolution reaction (OER). Although the commercialization of primary Zn-air batteries have been achieved for over 80 years, the rise of rechargeable ones is still in the early stages with a variety of technical hurdles.[14] Even with great improvements,[15–18] the relatively low energy efficiency is still an obstacle, which is caused by the low discharge voltages (i.e., <1.4 V)[19,20] and high charge voltages (i.e., >2.0 V).[21] Recently, remedies have been proposed through incorporating the redox reactions of transition metal into Zn-air batteries to offer improved working voltages. For example, Lee et al. reported a hybrid battery based on $NiO/Ni(OH)_2$ nanoflakes, which can initially deliver a discharge voltage of 1.7 V in the Zn-Ni reaction region and achieve a specific capacity of over 800 mAh g_{Zn}^{-1} from the Zn-air reaction.[22] Li et al. developed a $NiCo_2O_4$ nanowire-decorated nickel foam electrode, which enabled in a Zn-air battery to achieve a high voltage of 1.7 V due to the redox reaction and long cycle life of 5000 cycles.[23] Through using $MnCo_2O_4$ nanoparticles combined with nitrogen-doped reduced graphene oxide, Qaseem et al. demonstrated that a hybrid battery could present a high initial discharge voltage of 1.75 V and energy efficiency of 86% for 100 cycles.[24] However, the reported transition metal oxides with high pseudocapacitance exhibit limited ORR activity, leading to low operating voltages in Zn-air batteries (e.g., 1.0 V at 5 mA cm^{-2}).[23] In our previous

work, Co_3O_4 nanosheets grown on carbon cloth was used as the electrode and successfully combined Zn-Co_3O_4 and Zn-air batteries together, resulting in a working voltage up to 1.85 V and a specific capacity up to 792 mAh g_{Zn}^{-1}. In addition, the high energy efficiency of over 70% and high rate capabilities were demonstrated.[25] Whereas the utilization ratio of Co_3O_4 nanosheets in the Zn-Co_3O_4 reaction was poor (<10%), and the discharge voltage in the Zn-air reaction was low (e.g., <0.8 V) even at 10 mA cm^{-2}.[25,26] Moreover, the irreversible conversions of transition metal oxides in alkaline electrolytes occur during cycling, resulting in the degradation in both energy efficiency and cycling stability.[27,28]

The above-mentioned issues in conventional Zn-based batteries require novel solutions at the system level. Here we report a new type of hybrid battery that integrates a Zn-Ag and a Zn-air battery, in which Ag works first as the active reactant in the Zn-Ag reaction region, and then plays the role of an effective ORR catalyst in the Zn-air reaction region. On both electrodes, the corresponding electrochemical reactions can be described as:

Positive electrode:

$$2AgO + H_2O + 2e^- \underset{\text{Charge}}{\overset{\text{Discharge}}{\rightleftharpoons}} Ag_2O + 2OH^- \ (E = 0.61\,V\ vs.\,SHE) \quad (1)$$

$$Ag_2O + H_2O + 2e^- \underset{\text{Charge}}{\overset{\text{Discharge}}{\rightleftharpoons}} 2Ag + 2OH^- \ (E = 0.34\,V\ vs.\,SHE) \quad (2)$$

$$O_2 + 2H_2O + 4e^- \underset{\text{Charge}}{\overset{\text{Discharge}}{\rightleftharpoons}} 4OH^- \ (E = 0.40\,V\ vs.\,SHE) \quad (3)$$

Negative electrode:

$$Zn + 4OH^- \underset{\text{Charge}}{\overset{\text{Discharge}}{\rightleftharpoons}} Zn(OH)_4^{2-} + 4e^- (E = -1.25\,V\ vs.\,SHE) \quad (4)$$

The high discharge voltages come from the electrode reactions of a Zn-Ag battery, enabling high energy density, good power density, and improved energy efficiency. Additionally, the half-open feature of the Zn-air battery solves the oxygen evolution issue encountered in a conventional Zn-

Ag battery, leading to greatly improved cycling stability. Hence, the hybrid battery possesses the unique advantages of both battery systems. As a proof of concept, Zn-deposited carbon cloth was used as the negative electrode, while Ag and RuO_2 nanoparticle-decorated carbon nanotubes (RuO_2/CNT) were used as the positive electrode materials.[29] A hybrid battery was first built using an alkaline electrolyte solution to evaluate the electrochemical performances under different operating conditions. Further, a flexible battery based on a gel electrolyte was constructed to test the stability under various mechanical deformations.

2. Results and Discussion

Figure 1 presents the characteristics of the electrode materials. The Zn negative electrode was fabricated through electrodeposition of Zn on the carbon fibers as reported before.[30] As seen from the scanning electron microscopy (SEM) image in **Figure 1a** inset, the Zn plates (about 1 μm in diameter) are distributed uniformly on the carbon fiber surface. The phase purity of the Zn electrode is confirmed by the X-ray diffraction (XRD) pattern (**Figure 1b**); all peaks correspond well to those for Zn (JCPDS # 87-0713). The use of electrodeposited Zn instead of metallic Zn foil or zinc powder-cohered with binder increases the surface area of the electrode (Figure S1),[31] minimizing the tendency of Zn dendrite formation during charging.[32] In addition, the flexible carbon cloth substrate is essential for the application of flexible batteries.[33] For the positive electrode, Ag particles with an average size of ~60 nm (Figure S2) and the surface area of 8.74 $m^2\ g^{-1}$ (Figure S3) are used as the active material. **Figure 1c** shows the transmission electron microscopy (TEM) image, in which the lattice fringes of 0.204 and 0.236 nm are ascribed to the (200) and (111) planes of Ag (JCPDS # 87-0597), respectively, and the peaks from the XRD pattern in **Figure 1d** well match those of Ag. The electrochemical properties tested in the 0.1 M KOH solution demonstrate that Ag is a good ORR catalyst with a four-electron transfer process

(Figure S4). However, the oxidation occurs in the OER process, and a poor activity is exhibited. Hence, a catalyst with high OER activity should be applied to facilitate the charge process. Although cost-effective OER catalysts such as transition-metal oxides (e.g., Co_3O_4) can be potentially applied,[15–18,34,35] here we use RuO_2 as a demonstration of this concept. The TEM image of the prepared RuO_2/CNT is shown in **Figure 1e**. RuO_2 nanoparticles are loaded on the CNT surface with a mean particle size of 6.7 nm (Figure S2). The high-resolution TEM result (**Figure 1e** inset) shows RuO_2 nanoparticles loaded multi-walled carbon nanotube, and the uniform interplanar spacing of 0.225 nm is due to the (200) plane of RuO_2 (JCPDS # 88-0286). From the XRD pattern in **Figure 1f**, the peaks corresponding to RuO_2 are clearly observed, and so are the peaks assigned to carbon. From the thermogravimetric analysis, the loading of RuO_2 is determined to be 13.1% (Figure S3). Attributed to the high surface area (99.02 $m^2\ g^{-1}$) and the high OER activity in the alkaline solution (Figure S4),[36] the inclusion of RuO_2/CNT will enhance the performance of the hybrid battery.

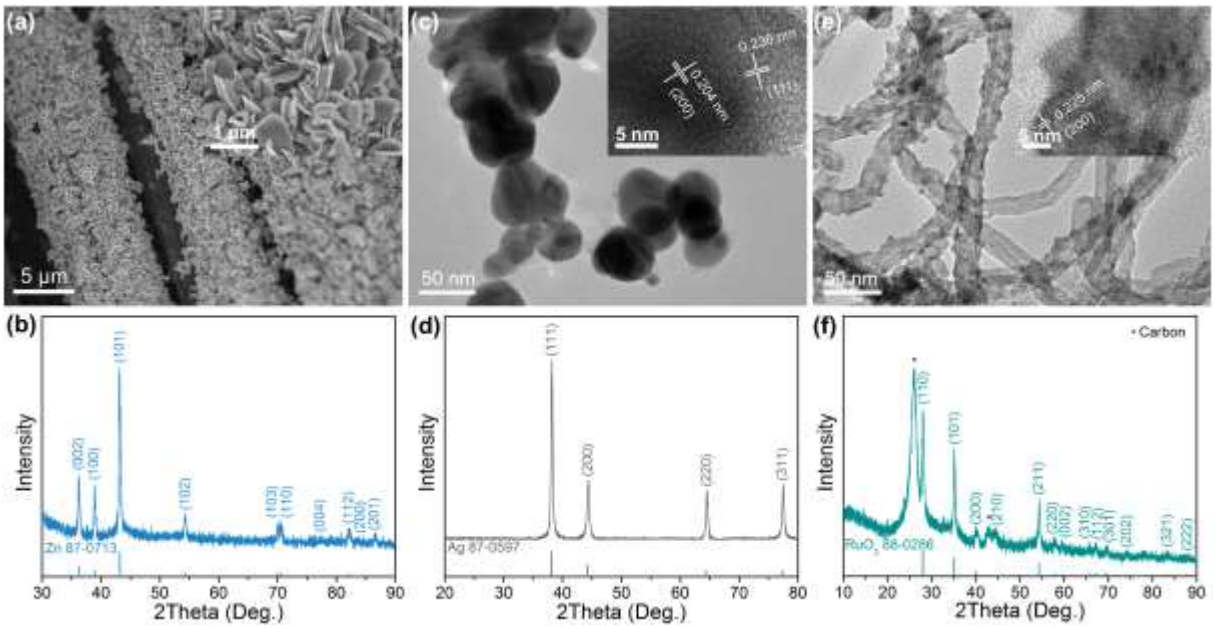

Figure 1. Characterization of the electrode materials applied in the hybrid battery: (a) SEM image of the Zn deposited carbon cloth, the inset shows the high-magnification of the Zn deposited surface. (b) XRD pattern of the Zn deposited carbon cloth. (c) TEM image of Ag powder, the corresponding lattice fringes are illustrated in the inset. (d) XRD pattern of Ag powder. (e) TEM image of RuO_2/CNTs, the lattice fringe of a RuO_2 particle on the CNT surface is shown in the inset. (f) XRD pattern of RuO_2/CNTs.

Figure 2a illustrated the cell configuration and the corresponding discharge and charge processes of a hybrid battery. The open circuit voltage (OCV) was 1.48 V, which corresponds to the equilibrium potential of 1.65 V between Zn and O_2.[14] To evaluate the galvanodynamic response, the battery was discharged from 0 to 200 mA cm^{-2} and charged till the cell voltage reached 2.5 V. As shown in **Figure 2b**, for the initial discharge, only one process corresponding to the ORR was observed, and a maximum power density of 91.9 mW cm^{-2} was obtained at 157 mA cm^{-2}. This high ORR performance may come from the synergistic effect of Ag and RuO_2/CNT, achieving a higher power density than that of the battery with Ag and CNT (Figure S5). During the charge, interestingly, three distinct voltage steps were observed. The voltage below 1.8 V and the second one near 2.0 V correspond to the oxidation of Ag, and the voltages above 2.2 V correspond to OER. After charging, three voltage steps corresponding to the reduction of AgO (AgO→Ag_2O→Ag) and the ORR were witnessed (Figure S6). Hence, these charge/discharge voltage profiles agree well with the previous results on rechargeable Zn-Ag and Zn-air batteries,[11,37] and the stepwise voltage profiles clearly show the distinct feature of the electrochemical systems. After the charge, the battery was galvanostatically discharged at the current densities of 2, 4, and 8 mA cm^{-2} (**Figure 2c**). **Figure 2c** inset clearly demonstrates the three discharge voltage plateaus. The first two high voltage plateaus near 1.85 V and 1.53 V

correspond to the discharge behavior of the Zn-Ag battery.[11] From the theoretical capacity of Ag in this work (0.9924 mAh cm^{-2}), the utilization ratio of Ag is calculated to be around 60% (Experimental section, Supporting Information), much higher than that of Co_3O_4 nanosheets in our previous work (<10%).[25] When AgO is reduced in the Zn-Ag battery, the produced Ag works as an ORR catalyst in the Zn-air battery, which delivers the voltage plateaus of 1.25, 1.20, and 1.15 V, respectively. The corresponding capacities at 2, 4, and 8 mA cm^{-2} are 800, 785, 764 mAh g_{Zn}^{-1}, respectively, approximate to the theoretical capacity of Zn (820 mAh g_{Zn}^{-1}). Based on the loading of Ag and the Zn consumed during discharge, the energy densities are estimated to be 944, 885, and 831 Wh kg^{-1}, respectively. Thus, the hybrid battery demonstrates the features of both high initial discharge voltages (1.85 V and 1.53 V) from the Zn-Ag battery and a high capacity from the Zn-air battery. It is noticed that sufficient Zn was provided during the discharge test, so that the capacity came from the Zn-air battery was much higher than that came from the reduction of AgO (Table S1). In practical applications where the amount of Zn is limited (e.g., fixed capacity as a rechargeable battery), the capacity contribution from the Zn-Ag battery can be larger as we demonstrated in the cycling test.

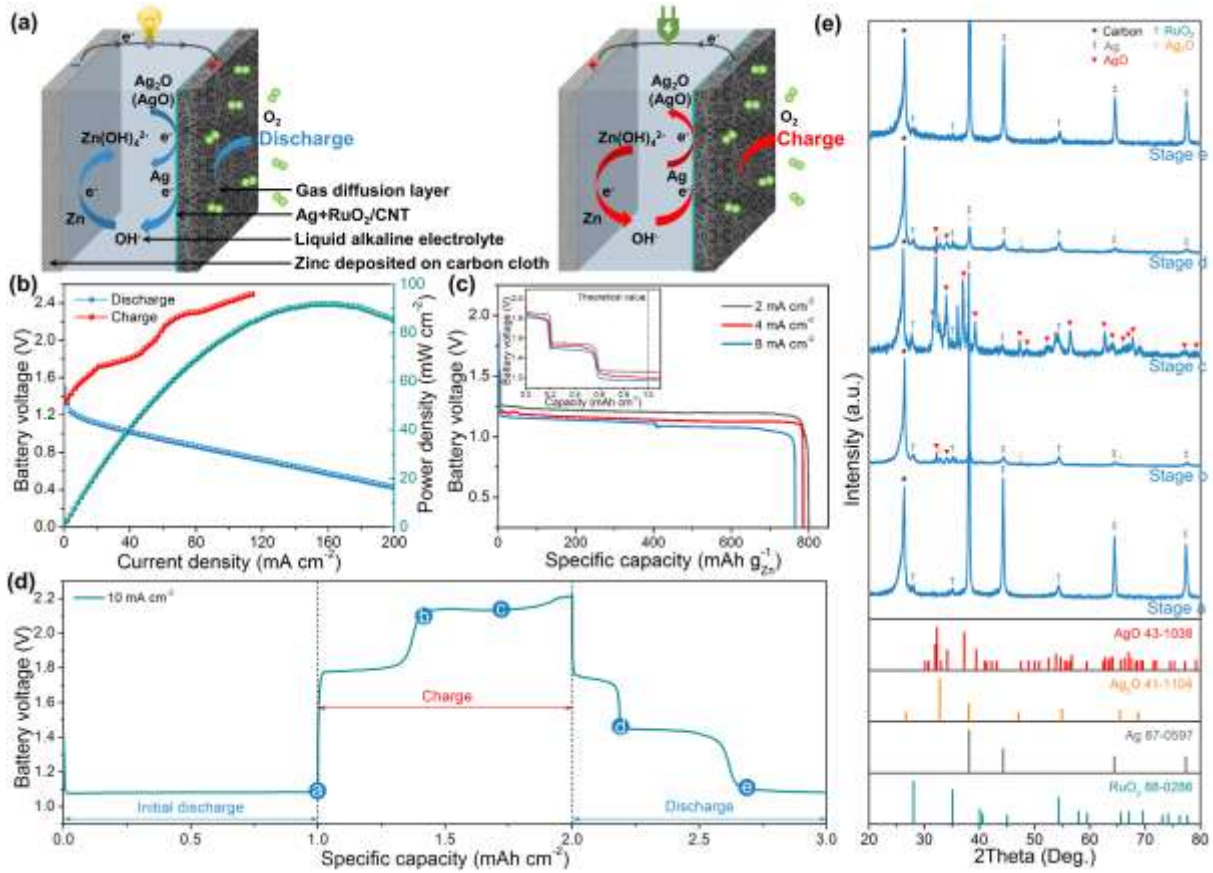

Figure 2. Electrochemical evaluation of the liquid electrolyte-based hybrid battery. (a) Scheme of the battery structure with proposed electrochemical processes during discharge and charge. (b) Discharge and charge polarization and the corresponding power density. (c) Galvanostatical discharge profiles at the current densities of 2, 4, and 8 mA cm^{-2} after the charge polarization, the inset shows the initial voltage profiles. (d) Initial discharge-charge-discharge voltage profiles at 10 mA cm^{-2}. (e) XRD patterns of the electrode at different states.

To prove the above-proposed electrochemical reactions of this hybrid battery during charge and discharge, a battery was discharged and charged at 10 mA cm^{-2} galvanostatically (**Figure 2d**), and the states marked from a to e were examined by ex-situ XRD, as shown in **Figure 2e**. In the first discharge region, a voltage plateau at about 1.08 V was observed, corresponding to the ORR of a typical Zn-air battery, and only Ag and RuO_2/CNT could be detected from the XRD

pattern acquired in state a. In the subsequent charge process, a voltage plateau was first observed at 1.78 V and then at 2.10 V (state b). At the same time, the intensities of the XRD peaks corresponding to Ag at 44.3°, 64.4°, and 77.4° decreased significantly as new peaks corresponding to Ag_2O at 32.8° and 47.0° appeared, together with some peaks corresponding to AgO. Hence, the first charge is dominated by the oxidation of Ag to form Ag_2O. When further charging the battery, another voltage plateau appeared at 2.14 V, and the voltage shows a little bit decrease till reaching state c. From the XRD result, the peaks corresponding to AgO with high intensities appear, indicating the further oxidation of Ag_2O to form AgO. After that, the charge voltage gradually increases until the end of charge, which may be caused by the decreased reaction sites due to the coverage of gaseous oxygen.[23] For the subsequent discharge process, similar to the voltage profiles in **Figure 2c**, three voltage steps were observed. After the voltage drop of the first plateau (state d), most XRD peaks corresponding to AgO disappeared, and the peaks correspond to Ag_2O (at 32.8°, 38.0°, and 47.1°) reappeared, indicating the reduction of AgO to Ag_2O. Then, another voltage plateau was observed at 1.44 V, after which the voltage quickly dropped to 1.08 V, as Ag_2O was fully converted to Ag according to the XRD result (state e). Hence, the reversible reactions between Ag and AgO associated with the OER and ORR occur in the charge and discharge processes, in which Ag acts as the active reactant as well as the catalyst for the ORR, while RuO_2/CNT acts as the effective OER catalyst, enabling the feasibility of this hybrid battery.

The rate performance of this battery was evaluated through charge and discharge at 2, 4, 8, 16, and 20 mA cm^{-2} with a constant capacity of 1.33 mAh cm^{-2}, and the results are shown in **Figure 3a**. Interestingly, only two charge voltage plateaus were observed at low current densities (2 and 4 mA cm^{-2}); accordingly, a two-step discharge voltage profile at the plateaus of around

1.5 V and 1.2 V was obtained, due likely to the high activity of RuO_2/CNT, which leads to a charge voltage of ~1.95 V for the OER. As a result, the OER process follows the oxidation of Ag to Ag_2O, preventing its further conversion to AgO at high voltages (e.g., >2.0V), which is consistent with the cyclic voltammetric (CV) results (Figure S7). In comparison, for the batteries with the electrodes composed of Ag or Ag with the addition of CNT, after the oxidation of Ag at ~1.65 V, the voltages quickly rise to 2.05 V to further oxidize Ag_2O to form AgO, and then increase to ~2.20 V for the OER. Consequently, stepwise voltage profiles with three plateaus are observed (Figure S8). When the current density further reaches 8 mA cm^{-2}, the charge voltage rises to 2.01 V after the first charge voltage plateau and decreases a little to 2.0 V in the OER region. For the subsequent discharge process, a short voltage plateau corresponding the reduction of AgO to Ag_2O appeared at 1.81 V. The similar phenomena appeared at higher current densities (16 and 20 mA cm^{-2}), and longer first discharge voltage plateaus were observed, indicating that a high charge voltage is needed to further oxidize Ag_2O,[11] and the utilization ratio of Ag can be improved to 70.3% at 20 mA cm^{-2} (Figure S9).

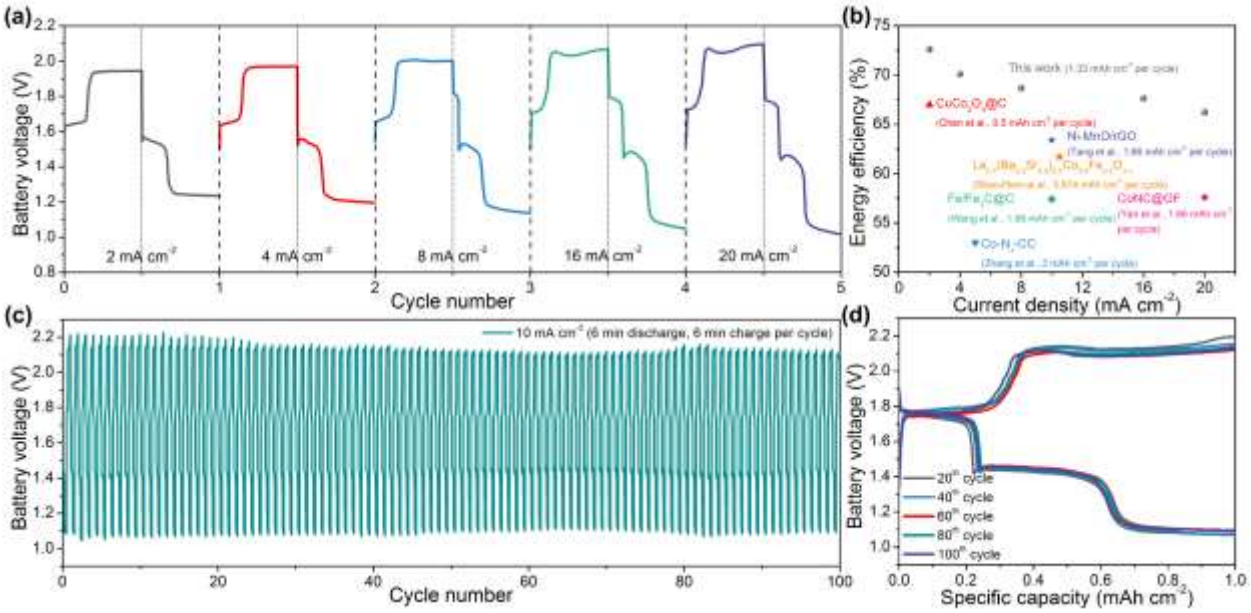

Figure 3. Rate and cycling performance of the hybrid battery based on the liquid electrolyte. (a) Voltage profiles at various current densities. (b) Corresponding energy efficiency, and the results from recently developed catalysts are listed for comparisons. (c) Long-term cycling stability at 10 mA cm^{-2} with a constant capacity of 1 mAh cm^{-2} (6 min for discharge and 6 min for charge). (d) Voltage profiles of selected cycles.

In practice, the energy efficiency is computed as the ratio of the energy delivered in discharge to that consumed in charge. Generally, to avoid the failure of reaction boundaries, a fixed capacity during cycling is applied in rechargeable metal-air batteries.[38,39] For example, in Li-air batteries, a given capacity of 1000 mAh $g_{catalyst}^{-1}$ is usually employed for testing.[40–42] In this work, due to the low overpotentials for the transition between Ag and its oxides (Ag_2O and AgO) and the high ORR and OER activity of Ag and RuO_2/CNT, the energy efficiency reaches 72.6%, 70.1%, 68.7%, 67.6%, and 66.2% at the current densities of 2, 4, 8, 16, 20 mA cm^{-2}, respectively. As compared in **Figure 3b**, this hybrid battery achieved higher energy efficiency than conventional Zn-air batteries with state-of-the-art catalysts developed recently [43–48] and the reported hybrid Zn batteries (Figure S10 and Table S2),[22–24] demonstrating the energy-saving feature of this battery through the combination of two distinct electrochemical systems.

The electrochemical stability was tests by discharge-charge cycles at different conditions and current densities. When cycled at 2 mA cm^{-2} within the voltage ranging from 1.3 V to 1.9 V in the Zn-Ag_2O battery region, due to the insufficient reduction of Ag_2O during discharge and oxidation of Ag during charge, the capacity retention drops to 72.0% after 198 cycles (Figure S11). Interestingly, after fully discharging the battery to the ORR region (1.07 V) and charging it to the OER region (2.04 V), the discharge capacity retention recovers to 83.7%. Even after 500 cycles, the capacity retention could still reach 55.7%. When operated as a hybrid battery at a

small current density of 4 mA cm^{-2}, stable voltage profiles ranging from 1.20 to 1.97 V were delivered for 100 cycles, resulting in the stable energy efficiency of 70% (Figure S12). In comparison, the battery with the Ag-based electrode exhibited a lower discharge voltage of 1.16 V and a higher charge voltage of 2.19 V for 100 cycles, resulting in the energy efficiency of ~60%. Although the addition of CNT improves the discharge and charge performance in the initial cycles, due to the lack of the OER activity, the high charge voltage causes the carbon corrosion and eventually decrease the cycling stability,[49] resulting in the drop of the energy efficiency from 69% to 53% after 100 cycles. Since the small current only induce the reaction between Ag and Ag_2O (Figure S8), we further test the cycling stability at a high current density of 10 mA cm^{-2} (6 min for discharge and 6 min for charge). As shown in **Figure 3c**, the battery maintained stable discharge and charge voltages of 1.08 and 2.15 V over 100 cycles after several initial cycles, and the energy efficiency kept at around 68% (Figure S13). At such a high current density, Ag can be fully oxidized to AgO. As illustrated in **Figure 3d**, three-step voltage profiles are observed throughout the cycling tests. The decreased charge voltages in the initial 20 cycles may be caused by the improved surface wetting of the electrode through electrochemical oxidation and reduction reactions, which improves accessibility of electrolyte to the electroactive sites.[23] For the discharge process, impressively, the three-step voltage profiles are almost maintained through 100 cycles, indicating the excellent reversibility of electrochemical reactions in this hybrid battery. Consequently, the capacity retention of Zn-AgO reaction is almost maintained 100%, which is excellent among the reported Zn-Ag batteries (Table S3).[11,37,50–53] Hence, linking the reactions of Zn-Ag batteries to the Zn-air batteries improves the oxidation efficiency of Ag, and the charge states (e.g., charge to Ag_2O or AgO) can be controlled by using effective OER catalysts, which together lead to the excellent stability of the hybrid battery.

Besides the well-coupled electrochemical reactions, using Zn deposited carbon cloth electrode instead of the metallic Zn plate may be another reason.[32] After 100 cycles, we examined both positive and negative electrodes. The morphology of the Ag loaded electrode is similar to the pristine one, and the Ag content remains almost the same (Figure S14). In addition, the morphology of the Zn electrode surface is well maintained (Figure S15). Due to the half-open design of the hybrid battery system, CO_2 in the ambient air can enter the battery, decreasing the ionic conductivity of the electrolyte.[54] In addition, the evaporation of liquid solvent (H_2O) occurs in the long-term operation, decreasing the reaction boundaries.[13] Both of these can increase the impedance and affect the electrochemical performance in the long-term operation (Figure S11). To this end, functional membranes that can select oxygen from ambient air and suppress the liquid electrolyte evaporation are essential for the practical applications of half-open battery systems.[55,56]

To provide power for the wearable and flexible electronic devices such as smart watches and flexible displays,[33] a quasi-solid-state hybrid battery was built (Experimental section, Supporting Information) for a proof-of-concept, and the structure is schematically shown in **Figure 4a**. Based on the carbon cloth substrate with high flexibility,[57] the Zn deposited and active materials (Ag and RuO_2/CNT) coated carbon cloth was used as the negative and positive electrode, respectively, between which was a gel electrolyte membrane. To pack these components and offer oxygen transport pathways, breathable tapes were used (Figure S16). **Figure 4b** shows the photograph of the assembled battery. An OCV of 1.45 V is presented, similar to the value of the battery using the liquid electrolyte (**Figure 2d**). The discharge and charge polarization curves are shown in **Figure 4c**, from which the overpotentials are larger due to the limited reaction boundaries.[13,33] At 60.8 mA cm^{-2}, the power density reaches the

maximum value of 30.5 mW cm^{-2}, higher than some reported solid-state Zn-air batteries.[44,58,59] The charge polarization curve also exhibits three distinct steps, resulting in the three discharge voltage steps corresponding to the reduction of AgO (AgO→Ag_2O→Ag) and the ORR (Figure S17). The rate performance of the flexible battery was evaluated through charge and discharge at 2, 4, 6, 8, and 10 mA cm^{-2} with a fixed capacity of 0.8 mAh cm^{-2}. Different from the liquid electrolyte-based battery, a three-step discharge voltage profile is presented even at the low current density of 2 mA cm^{-2}, as presented in **Figure 4d**, This may be attributed to the limited reaction boundaries due to the immobilized gel electrolyte.[13] which results in non-uniform overpotentials in the electrode during charge. At some reaction sites, the high charge potentials further oxidize Ag_2O to AgO, leading to the voltage plateau corresponding to the reduction of AgO during discharge. With increasing the current density, on the one hand, the resultant high charge voltage can further oxidize Ag_2O to AgO, increasing the energy storage; on the other side, high current densities cause large polarization during discharge, decreasing the voltage plateaus and the capacities of the Zn-Ag battery. The utilization ratio of Ag in the gel electrolyte-based battery is around 35%, lower than that in the battery with the liquid electrolyte (Figure S18), indicating the insufficient contact between the electrode materials and the electrolyte. From the charge-discharge performance, the energy efficiency is calculated to be 71.8%, 68.7%, 65.7%, 62.3%, and 60.2%, respectively (**Figure 4e**).[44] Owing to the high discharge voltage of AgO reduction (~1.8 V), a red light-emitting diode (LED) can be powered by just one single battery (**Figure 4e** inset), demonstrating its advantages of high operating voltage for electronic devices. The battery was further tested by discharge-charge cycling at 8 mA cm^{-2} (**Figures 4f** and **4g**). The three-step voltage profiles present from the second cycle, and exhibit similar shapes afterward. In addition, the discharge and charge voltages are in the range of 1.05 to 2.1 V for the

30 cycles, indicating good rechargeability and stability. Moreover, the end-to-end distance of the battery was changed from the initial 3.0 cm to 1.0 cm.[60] As presented in **Figure 4h**, the voltage profiles are almost identical under both flat and bending conditions, indicating the potential applications for wearable and flexible electronic devices.

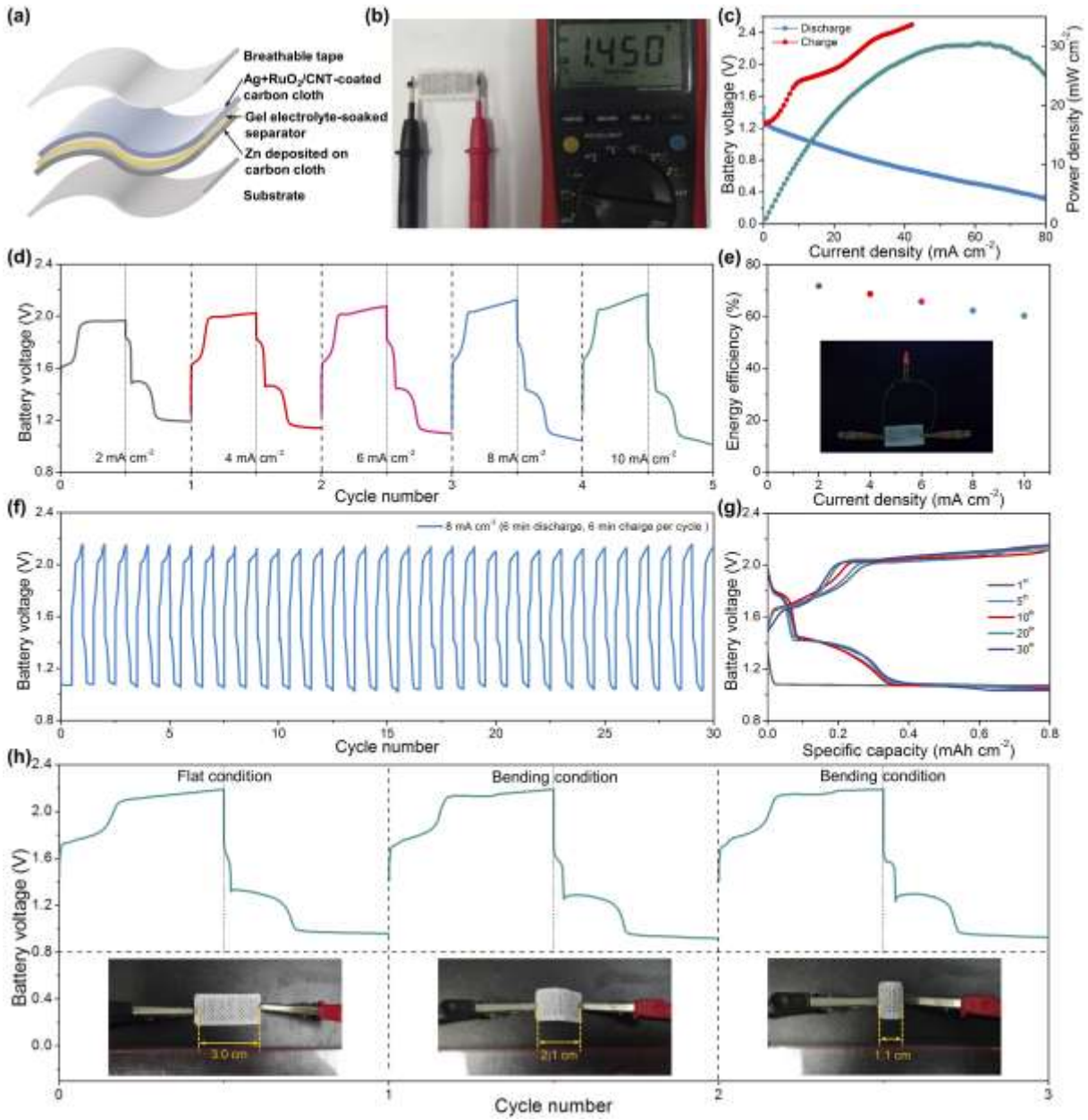

Figure 4. Electrochemical performance of the gel electrolyte-based hybrid battery. (a) Scheme of the flexible battery structure. (b) Photograph of the assembled flexible battery, and an OCV of

1.45 V is demonstrated. (c) Polarization and the power density. (d) Voltage profiles at different current densities. (e) The corresponding energy efficiency, and the inset photograph shows the flexible hybrid battery that lights up a red LED (1.7−2.3 V). (f) Cycling stability at 8 mA cm^{-2} (6 min for discharge and 6 min for charge). (g) Voltage profiles of the selected cycles. (h) Charge-discharge voltage profiles at 10 mA cm^{-2} (6 min for charge and 6 min for discharge) at different deformations.

For this hybrid battery, the stepwise low charge voltages and high discharge voltages result in the higher energy efficiency than conventional Zn-air batteries. Additionally, the half-open structure solves the oxygen evolution issue in conventional Zn-Ag batteries, leading to a greatly improved cycling stability. The impressive performance is contributed from the well-linked electrochemical reactions through a combination of Zn-Ag and Zn-air batteries with functional electrode materials. In the positive electrode, Ag works as the active reactant in the Zn-Ag reaction, which then plays the role of an effective ORR catalyst in the Zn-air reaction, coupling the discharge behaviors through these two distinct electrochemical systems. Since Ag will be oxidized during charge, RuO_2/CNTs are added to facilitate the charge process. On the one side, CNTs change the condition of Ag nanoparticles and offer electron transport pathways, improving the charge performance and the utilization ratio of Ag. On the other side, RuO_2 nanoparticle works as an effective OER catalyst, lowing the charge voltage and offering the possibilities of tuning the battery behaviors (e.g., the transition between Ag and Ag_2O/AgO). In the negative electrode, Zn particles grow in-situ on the carbon cloth, which provides large surface areas and suppresses the dendrite, enabling the long-term operating safety. Future work is undergoing to develop effective non-precious OER catalysts,[61,62] optimize the amount of active materials, improve the utilization ratio of Ag, and design novel battery structures with high durability.

3. Conclusions

In conclusion, a hybrid battery has been constructed to make good use of the unique advantages of a Zn-Ag battery and a Zn-air battery. It first exhibits two-step high discharge voltage plateaus of 1.85 V and 1.53 V (the discharge process of a Zn-Ag battery), after which the formed Ag particles function as an effective ORR catalyst, showing a discharge voltage plateau of 1.25 V (the discharge process of a Zn-air battery). The combination of the voltages of the Zn-Ag reactions and the capacity of the Zn-air reaction results in a remarkable energy density of 944 Wh kg^{-1} based on the weight of Ag and consumed Zn. Attributed to the low overpotentials for the transition between Ag and its oxides (Ag_2O and AgO) and the high ORR and OER activity of Ag and RuO_2/CNT, respectively, the energy efficiency of this hybrid battery at the current densities of 2, 4, 8, 16, 20 mA cm^{-2} reaches 72.6%, 70.1%, 68.7%, 67.6%, and 66.2%, respectively, superior to that of conventional Zn-air batteries. The half-open structure of this hybrid battery solves the oxygen evolution issue in conventional Zn-Ag batteries, resulting in excellent reversibility and stability. At 10 mA cm^{-2}, the hybrid battery can maintain the high energy efficiency of 68% and the capacity retention of nearly 100% through 100 cycles, outperforming both conventional Zn-air or Zn-Ag batteries and reported hybrid Zn batteries. In addition, a gel electrolyte-based flexible battery is assembled as a demonstration, which displays not only high power density, energy efficiency, and cycling stability, but also stable performance under various mechanical deformations. The stellar performance is attributed to the integration of the electrochemical reactions of two distinct battery systems. The work also inspires the explorations of novel hybrid energy storage systems with excellent performance for electric vehicles and flexible electronic devices.

ASSOCIATED CONTENT

Supporting Information

The following file is available free of charge.

Experimental methods, SEM image of Ag powder, nitrogen adsorption-desorption isotherms and the pore distribution, thermogravimetric analysis, electrochemical properties of Ag and RuO_2/CNT, voltage profiles of the batteries with Ag-based electrode materials, photographs of the components of the gel electrolyte-based flexible battery, and performance comparisons with reported works (PDF)

AUTHOR INFORMATION

Corresponding Author

*E-mail: zongping.shao@curtin.edu.au (Zongping Shao)

*E-mail: meng.ni@polyu.edu.hk (Meng Ni)

ORCID

Peng Tan: 0000-0001-5750-0477

Meilin Liu: 0000-0002-6188-2372

Zongping Shao: 0000-0002-4538-4218

Meng Ni: 0000-0001-5310-4039

Notes

The authors declare no competing financial interest.

ACKNOWLEDGMENT

P. Tan thanks the funding support from CAS Pioneer Hundred Talents Program. M. Ni thanks the funding support from The Hong Kong Polytechnic University (G-YBJN and G-YW2D) and a

grant (Project Number: PolyU 152214/17E) from Research Grant Council, University Grants Committee, Hong Kong SAR.

REFERENCES

(1) Dunn, B.; Kamath, H.; Tarascon, J.-M. Electrical Energy Storage for the Grid: A Battery of Choices. *Science* **2011**, *334*, 928–935.

(2) Wang, Z.-L.; Xu, D.; Xu, J.-J.; Zhang, X.-B. Oxygen Electrocatalysts in Metal-Air Batteries: From Aqueous to Nonaqueous Electrolytes. *Chem. Soc. Rev.* **2014**, *43*, 7746–7786.

(3) Cairns, E. J.; Albertus, P. Batteries for Electric and Hybrid-Electric Vehicles. *Annu. Rev. Chem. Biomol. Eng.* **2010**, *1*, 299–320.

(4) Yu, M.; Wang, Z.; Han, Y.; Tong, Y.; Lu, X.; Yang, S. Recent Progress in the Development of Anodes for Asymmetric Supercapacitors. *J. Mater. Chem. A* **2016**, *4*, 4634–4658.

(5) Fu, K. K.; Cheng, J.; Li, T.; Hu, L. Flexible Batteries: From Mechanics to Devices. *ACS Energy Lett.* **2016**, *1*, 1065–1079.

(6) Pan, H.; Shao, Y.; Yan, P.; Cheng, Y.; Han, K. S.; Nie, Z.; Wang, C.; Yang, J.; Li, X.; Bhattacharya, P.; Mueller, K.; Liu, J. Reversible Aqueous Zinc/manganese Oxide Energy Storage from Conversion Reactions. *Nat. Energy* **2016**, *1*, 16039.

(7) Gong, M.; Li, Y.; Zhang, H.; Zhang, B.; Zhou, W.; Feng, J.; Wang, H.; Liang, Y.; Fan, Z.; Liu, J.; Dai, H. Ultrafast High-Capacity NiZn Battery with NiAlCo-Layered Double Hydroxide. *Energy Environ. Sci.* **2014**, *7*, 2025–2032.

(8) McLarnon, F. R.; Cairns, E. J. The Secondary Alkaline Zinc Electrode. *J. Electrochem. Soc.* **1991**, *138*, 645–656.

(9) Yan, C.; Wang, X.; Cui, M.; Wang, J.; Kang, W.; Foo, C. Y.; Lee, P. S. Stretchable Silver-Zinc Batteries Based on Embedded Nanowire Elastic Conductors. *Adv. Energy Mater.* **2014**, *4*, 1301396.

(10) Karpinski, A. P.; Makovetski, B.; Russell, S. J.; Serenyi, J. R.; Williams, D. C. Silver–Zinc : Status of Technology and Applications. *J. Power Sources* **1999**, 80, 53–60.

(11) Ozgit, D.; Hiralal, P.; Amaratunga, G. A. J. Improving Performance and Cyclability of Zinc-Silver Oxide Batteries by Using Graphene as a Two Dimensional Conductive Additive. *ACS Appl. Mater. Interfaces* **2014**, *6*, 20752–20757.

(12) Zhang, L.; Chen, L.; Zhou, X.; Liu, Z. Towards High-Voltage Aqueous Metal-Ion Batteries Beyond 1.5 V: The Zinc/Zinc Hexacyanoferrate System. *Adv. Energy Mater.* **2015**, *5*, 1400930.

(13) Fu, J.; Cano, Z. P.; Park, M. G.; Yu, A.; Fowler, M.; Chen, Z. Electrically Rechargeable Zinc-Air Batteries: Progress, Challenges, and Perspectives. *Adv. Mater.* **2017**, *29*, 1604685.

(14) Li, Y.; Dai, H. Recent Advances in Zinc–air Batteries. *Chem. Soc. Rev.* **2014**, *43*, 5257–5275.

(15) Pei, P.; Wang, K.; Ma, Z. Technologies for Extending Zinc-Air Battery's Cyclelife: A Review. *Appl. Energy* **2014**, *128*, 315–324.

(16) Wang, Z.-L.; Xu, D.; Xu, J.-J.; Zhang, X.-B. Oxygen Electrocatalysts in Metal–air Batteries: From Aqueous to Nonaqueous Electrolytes. *Chem. Soc. Rev.* **2014**, *43*, 7746–7786.

(17) Suen, N.-T.; Hung, S.-F.; Quan, Q.; Zhang, N.; Xu, Y.-J.; Chen, H. M. Electrocatalysis for the Oxygen Evolution Reaction: Recent Development and Future Perspectives. *Chem. Soc.*

Rev. **2017**, *46*, 337–365.

(18) Caramia, V.; Bozzini, B. Materials Science Aspects of Zinc–air Batteries: A Review. *Mater. Renew. Sustain. Energy* **2014**, *3*, 28.

(19) Li, Y.; Gong, M.; Liang, Y.; Feng, J.; Kim, J. E.; Wang, H.; Hong, G.; Zhang, B.; Dai, H. Advanced Zinc-Air Batteries Based on High-Performance Hybrid Electrocatalysts. *Nat Commun* **2013**, *4*, 1805.

(20) Jung, J.-I.; Risch, M.; Park, S.; Kim, M. G.; Nam, G.; Jeong, H.-Y.; Shao-Horn, Y.; Cho, J. Optimizing Nanoparticle Perovskite for Bifunctional Oxygen Electrocatalysis. *Energy Environ. Sci.* **2016**, *9*, 176–183.

(21) Lee, D. U.; Xu, P.; Cano, Z. P.; Kashkooli, A. G.; Park, M. G.; Chen, Z. Recent Progress and Perspectives on Bi-Functional Oxygen Electrocatalysts for Advanced Rechargeable Metal–air Batteries. *J. Mater. Chem. A* **2016**, *4*, 7107–7134.

(22) Lee, D. U.; Fu, J.; Park, M. G.; Liu, H.; Ghorbani Kashkooli, A.; Chen, Z. Self-Assembled NiO/$Ni(OH)_2$ Nanoflakes as Active Material for High-Power and High-Energy Hybrid Rechargeable Battery. *Nano Lett.* **2016**, *16*, 1794–1802.

(23) Li, B.; Quan, J.; Loh, A.; Chai, J.; Chen, Y.; Tan, C.; Ge, X.; Hor, T. S. A.; Liu, Z.; Zhang, H.; Zong, Y. A Robust Hybrid Zn-Battery with Ultralong Cycle Life. *Nano Lett.* **2017**, *17*, 156–163.

(24) Qaseem, A.; Chen, F.; Qiu, C.; Mahmoudi, A.; Wu, X.; Wang, X.; Johnston, R. L. Reduced Graphene Oxide Decorated with Manganese Cobalt Oxide as Multifunctional Material for Mechanically Rechargeable and Hybrid Zinc-Air Batteries. *Part. Part. Syst. Charact.* **2017**, *34*, 1700097.

(25) Tan, P.; Chen, B.; Xu, H.; Cai, W.; He, W.; Liu, M.; Shao, Z.; Ni, M. Co_3O_4 Nanosheets

as Active Material for Hybrid Zn Batteries. *Small* **2018**, *14*, 1800225.

(26) Tan, P.; Chen, B.; Xu, H.; Cai, W.; He, W.; Ni, M. Investigation on the Electrode Design of Hybrid Zn-Co_3O_4/air Batteries for Performance Improvements. *Electrochim. Acta* **2018**, *283*, 1028–1036.

(27) Wang, H.; Tang, Z.; Liu, Y.; Lee, C. Synthesis and Behavior of Al-Stabilized α-$Ni(OH)_2$. *Trans. Nonferrous Met. Soc. China* **2009**, *19*, 170–175.

(28) Kong, X.; Zhao, J.; Shi, W.; Zhao, Y.; Shao, M.; Wei, M.; Wang, L.; Duan, X. Fabrication of Aluminum-Doped α-$Ni(OH)_2$ with Hierarchical Architecture and Its Largely Enhanced Electrocatalytic Performance. *Electrochim. Acta* **2012**, *80*, 257–263.

(29) Jian, Z.; Liu, P.; Li, F.; He, P.; Guo, X.; Chen, M.; Zhou, H. Core-Shell-Structured CNT@RuO_2 Composite as a High-Performance Cathode Catalyst for Rechargeable Li-O_2 Batteries. *Angew. Chemie - Int. Ed.* **2014**, *53*, 442–446.

(30) Yu, M.; Wang, Z.; Hou, C.; Wang, Z.; Liang, C.; Zhao, C.; Tong, Y.; Lu, X.; Yang, S. Nitrogen-Doped Co_3O_4 Mesoporous Nanowire Arrays as an Additive-Free Air-Cathode for Flexible Solid-State Zinc-Air Batteries. *Adv. Mater.* **2017**, *29*, 1602868.

(31) Hiralal, P.; Imaizumi, S.; Unalan, H. E.; Matsumoto, H.; Minagawa, M.; Rouvala, M.; Tanioka, A.; Amaratunga, G. A. J. Nanomaterial-Enhanced All-Solid Flexible Zinc−Carbon Batteries. *ACS Nano* **2010**, *4*, 2730–2734.

(32) Wang, X.; Wang, F.; Wang, L.; Li, M.; Wang, Y.; Chen, B.; Zhu, Y.; Fu, L.; Zha, L.; Zhang, L.; Wu, Y.; Huang, W. An Aqueous Rechargeable Zn//Co_3O_4 Battery with High Energy Density and Good Cycling Behavior. *Adv. Mater.* **2016**, *28*, 4904–4911.

(33) Tan, P.; Chen, B.; Xu, H.; Zhang, H.; Cai, W.; Ni, M.; Liu, M.; Shao, Z. Flexible Zn– and Li–air Batteries: Recent Advances, Challenges, and Future Perspectives. *Energy Environ.*

Sci. **2017**, *10*, 2056–2080.

(34) Du, G.; Liu, X.; Zong, Y.; Hor, T. S. A.; Yu, A.; Liu, Z. Co_3O_4 Nanoparticle-Modified MnO_2 Nanotube Bifunctional Oxygen Cathode Catalysts for Rechargeable Zinc–air Batteries. *Nanoscale* **2013**, *5*, 4657–4661.

(35) Guan, C.; Sumboja, A.; Wu, H.; Ren, W.; Liu, X.; Zhang, H.; Liu, Z.; Cheng, C.; Pennycook, S. J.; Wang, J. Hollow Co_3O_4 Nanosphere Embedded in Carbon Arrays for Stable and Flexible Solid-State Zinc-Air Batteries. *Adv. Mater.* **2017**, *29*, 1704117.

(36) Tan, P.; Shyy, W.; Zhao, T. S.; Zhu, X. B.; Wei, Z. H. A RuO_2 Nanoparticle-Decorated Buckypaper Cathode for Non-Aqueous Lithium–oxygen Batteries. *J. Mater. Chem. A* **2015**, *3*, 19042–19049.

(37) Berchmans, S.; Bandodkar, A. J.; Jia, W.; Ramírez, J.; Meng, Y. S.; Wang, J. An Epidermal Alkaline Rechargeable Ag–Zn Printable Tattoo Battery for Wearable Electronics. *J. Mater. Chem. A* **2014**, *2*, 15788–15795.

(38) Lu, J.; Li, L.; Park, J. B.; Sun, Y. K.; Wu, F.; Amine, K. Aprotic and Aqueous Li-O_2 Batteries. *Chem. Rev.* **2014**, *114*, 5611–5640.

(39) Li, Y.; Lu, J. Metal–Air Batteries: Will They Be the Future Electrochemical Energy Storage Device of Choice? *ACS Energy Lett.* **2017**, *2*, 1370–1377.

(40) Tan, P.; Liu, M.; Shao, Z.; Ni, M. Recent Advances in Perovskite Oxides as Electrode Materials for Nonaqueous Lithium-Oxygen Batteries. *Adv. Energy Mater.* **2017**, *7*, 1602674.

(41) Lu, J.; Jung Lee, Y.; Luo, X.; Chun Lau, K.; Asadi, M.; Wang, H.-H.; Brombosz, S.; Wen, J.; Zhai, D.; Chen, Z.; Miller, D.; Sub Jeong, Y.; Park, J.; Zak Fang, Z.; Kumar, B.; Salehi-Khojin, A.; Sun, Y.; Curtiss, L.; Amine, K. A Lithium–oxygen Battery Based on

Lithium Superoxide. *Nature* **2016**, *529*, 1–7.

(42) Tan, P.; Shyy, W.; Wu, M. C.; Huang, Y. Y.; Zhao, T. S. Carbon Electrode with NiO and RuO_2 Nanoparticles Improves the Cycling Life of Non-Aqueous Lithium-Oxygen Batteries. *J. Power Sources* **2016**, *326*, 303–312.

(43) Jung, J.-I.; Risch, M.; Park, S.; Kim, M. G.; Nam, G.; Jeong, H.-Y.; Shao-Horn, Y.; Cho, J. Optimizing Nanoparticle Perovskite for Bifunctional Oxygen Electrocatalysis. *Energy Environ. Sci.* **2016**, *9*, 176–183.

(44) Tang, C.; Wang, B.; Wang, H. F.; Zhang, Q. Defect Engineering toward Atomic Co–N_x–C in Hierarchical Graphene for Rechargeable Flexible Solid Zn-Air Batteries. *Adv. Mater.* **2017**, *29*, 1–7.

(45) Wang, X.; Li, Y.; Jin, T.; Meng, J.; Jiao, L.; Zhu, M.; Chen, J. Electrospun Thin-Walled $CuCo_2O_4$@C Nanotubes as Bifunctional Oxygen Electrocatalysts for Rechargeable Zn-Air Batteries. *Nano Lett.* **2017**, *17*, 7989–7994.

(46) Liu, S.; Wang, M.; Sun, X.; Xu, N.; Liu, J.; Wang, Y.; Qian, T.; Yan, C. Facilitated Oxygen Chemisorption in Heteroatom-Doped Carbon for Improved Oxygen Reaction Activity in All-Solid-State Zinc-Air Batteries. *Adv. Mater.* **2018**, *30*, 1704898.

(47) Fu, G.; Yan, X.; Chen, Y.; Xu, L.; Sun, D.; Lee, J.-M.; Tang, Y. Boosting Bifunctional Oxygen Electrocatalysis with 3D Graphene Aerogel-Supported Ni/MnO Particles. *Adv. Mater.* **2018**, *30*, 1704609.

(48) Wang, Q.; Lei, Y.; Chen, Z.; Wu, N.; Wang, Y.; Wang, B.; Wang, Y. Fe/Fe_3C@C Nanoparticles Encapsulated in N-Doped graphene–CNTs Framework as an Efficient Bifunctional Oxygen Electrocatalyst for Robust Rechargeable Zn–air Batteries. *J. Mater. Chem. A* **2018**, *6*, 516–526.

(49) Ma, Z.; Pei, P.; Wang, K.; Wang, X.; Xu, H.; Liu, Y.; peng, G. Degradation Characteristics of Air Cathode in Zinc Air Fuel Cells. *J. Power Sources* **2015**, *274*, 56–64.

(50) Ullah, S.; Ahmed, F.; Badshah, A.; Ali Altaf, A.; Raza, R.; Lal, B.; Hussain, R. Solvothermal Preparation of ZnO Nanorods as Anode Material for Improved Cycle Life Zn/AgO Batteries. *PLoS One* **2013**, *8*, 1–7.

(51) Shin, J.; You, J.-M.; Lee, J. Z.; Kumar, R.; Yin, L.; Wang, J.; Shirley Meng, Y. Deposition of ZnO on Bismuth Species towards a Rechargeable Zn-Based Aqueous Battery. *Phys. Chem. Chem. Phys.* **2016**, *18*, 26376–26382.

(52) Zamarayeva, A. M.; Ostfeld, A. E.; Wang, M.; Duey, J. K.; Deckman, I.; Lechêne, B. P.; Davies, G.; Steingart, D. A.; Arias, A. C. Flexible and Stretchable Power Sources for Wearable Electronics. *Sci. Adv.* **2017**, *3*, e1602051.

(53) Kumar, R.; Shin, J.; Yin, L.; You, J.-M.; Meng, Y. S.; Wang, J. All-Printed, Stretchable Zn-Ag_2O Rechargeable Battery via Hyperelastic Binder for Self-Powering Wearable Electronics. *Adv. Energy Mater.* **2017**, *7*, 1602096.

(54) Fu, J.; Zhang, J.; Song, X.; Zarrin, H.; Tian, X.; Qiao, J.; Rasen, L.; Li, K.; Chen, Z. A Flexible Solid-State Electrolyte for Wide-Scale Integration of Rechargeable Zinc–air Batteries. *Energy Environ. Sci.* **2016**, *9*, 663–670.

(55) Tan, P.; Wei, Z. H.; Shyy, W.; Zhao, T. S.; Zhu, X. B. A Nano-Structured RuO_2/NiO Cathode Enables the Operation of Non-Aqueous Lithium–air Batteries in Ambient Air. *Energy Environ. Sci.* **2016**, *9*, 1783–1793.

(56) Wang, M.; Zhao, J.; Wang, X.; Liu, A.; Gleason, K. K. Recent Progress on Submicron Gas-Selective Polymeric Membranes. *J. Mater. Chem. A* **2017**, *5*, 8860–8886.

(57) Meng, F.; Zhong, H.; Bao, D.; Yan, J.; Zhang, X. In Situ Coupling of Strung Co_4N and

Intertwined N-C Fibers toward Free-Standing Bifunctional Cathode for Robust, Efficient, and Flexible Zn-Air Batteries. *J. Am. Chem. Soc.* **2016**, *138*, 10226–10231.

(58) Fu, J.; Lee, D. U.; Hassan, F. M.; Yang, L.; Bai, Z.; Park, M. G.; Chen, Z. Flexible High-Energy Polymer-Electrolyte-Based Rechargeable Zinc-Air Batteries. *Adv. Mater.* **2015**, *27*, 5617–5622.

(59) Yu, M.; Wang, Z.; Hou, C.; Wang, Z.; Liang, C.; Zhao, C.; Tong, Y.; Lu, X.; Yang, S. Nitrogen-Doped Co_3O_4 Mesoporous Nanowire Arrays as an Additive-Free Air-Cathode for Flexible Solid-State Zinc-Air Batteries. *Adv. Mater.* **2017**, *29*, 1602868.

(60) Mao, L.; Meng, Q.; Ahmad, A.; Wei, Z. Mechanical Analyses and Structural Design Requirements for Flexible Energy Storage Devices. *Adv. Energy Mater.* **2017**, *7*, 1700535.

(61) Chen, D.; Chen, C.; Baiyee, Z. M.; Shao, Z.; Ciucci, F. Nonstoichiometric Oxides as Low-Cost and Highly-Efficient Oxygen Reduction/Evolution Catalysts for Low-Temperature Electrochemical Devices. *Chem. Rev.* **2015**, *115*, 9869–9921.

(62) Huang, Z.-F.; Wang, J.; Peng, Y.; Jung, C.-Y.; Fisher, A.; Wang, X. Design of Efficient Bifunctional Oxygen Reduction/Evolution Electrocatalyst: Recent Advances and Perspectives. *Adv. Energy Mater.* **2017**, *7*, 1700544.

Table of content graphic